Translational Oncology 16 (2022) 101323

Contents lists available at ScienceDirect

Translational Oncology

journal homepage: www.elsevier.com/locate/tranon

Original Research

Defective transcription elongation in human cancers imposes targetable proteotoxic vulnerability

B. Muhammad [a,b], L.G. Parks [a], K. Komurov [b,c,1,*], L.M. Privette Vinnedge [a,c,*]

[a] Division of Oncology, Cancer and Blood Diseases Institute, Cincinnati Children's Hospital Medical Center, MLC7018, 3333 Burnet Avenue, Cincinnati, OH 45229, United States
[b] Division of Experimental Hematology and Cancer Biology, Cancer and Blood Diseases Institute, Cincinnati Children's Hospital Medical Center, Cincinnati, OH 45229, United States
[c] Department of Pediatrics, University of Cincinnati College of Medicine, Cincinnati, OH, United States

ARTICLE INFO

Keywords:
Transcription elongation defects (TE^{def})
Aggresomes
Protein homeostasis
Proteotoxic stress
Autophagy

ABSTRACT

Successful cancer therapy is contingent on identifying cancer-specific aberrant phenotypes and their associated vulnerabilities. We recently reported that a subset of almost every cancer type contains a genome-wide defect in RNA Polymerase II-mediated transcription elongation (TE^{def}), which impairs the expression of long genes and confers resistance to anti-tumor immune attack. Using a combination of computational analysis and laboratory experiments, we report that tumor cells with TE^{def} have widespread overexpression of the components of the protein homeostasis machinery (mostly composed of short genes), including protein folding and clearance. Accordingly, TE^{def} cells were characterized by abnormally high levels of insoluble protein aggregates in the cytoplasm and autophagy influx. We present evidence that TE^{def} cells exhibit impaired clearance of misfolded protein aggregates through the ubiquitin-proteasome system, and thus rely on autophagy for their degradation. As such, while these cells were highly resistant to proteasome inhibitors, they were acutely sensitive to inhibitors of autophagy *in vitro* and *in vivo*. This study reveals a major aberrant phenotype that is observed in ~15–25% of all cancers and characterizes a unique cellular vulnerability that can be readily exploited in the clinic to improve treatment efficacy.

Introduction

Maintaining protein homeostasis (proteostasis) is fundamental for cell survival. Cells deploy sophisticated multi-stage quality control processes to closely monitor steps of protein synthesis including transcription, translation, post-translational modifications, protein folding, and degradation. Each of these steps recruit specialized regulatory components of the proteostasis network in a temporal and spatial manner. To this end, protein synthesis is viewed as an intrinsically error prone process that requires tight regulation to ensure the production of functional proteins, while eliminating the defective ones (reviewed in [1–3]).

Defective protein products can be of various forms such as defective ribosomal proteins (DRiPs), rapidly degraded peptides (RDPs), intrinsically disordered proteins (IDPs), terminally misfolded proteins (soluble), toxic protein aggregates and aggresomes [4–6]. Accordingly, several quality control systems have been developed to ensure faithful protein production. Collectively, these systems aim to refold soluble misfolded polypeptides and degrade or sequester the terminally misfolded proteins (often insoluble) into distinct quality control compartments. Examples of such quality control strategies include ribosome quality control (RQC), unfolded protein response (UPR), ubiquitin proteasome system (UPS), endoplasmic reticulum associated degradation pathway (ERAD), autophagy, etc (reviewed in [4]).

UPS and autophagy are the major degradation pathways for terminally misfolded proteins and/or toxic protein aggregates. These two pathways often act interchangeably to maintain the proteostasis network [4]. Evidence suggests that impairment of the UPS triggers compensatory induction of autophagy [6] whereas autophagy inhibition leads to the accumulation of proteasomal substrates [7,8]. The capacity of UPS is limited to the degradation of soluble and/or monomeric polyubiquitinated peptides [5]. Importantly, during the process of

* Corresponding authors: Department of Pediatrics, University of Cincinnati College of Medicine, Cincinnati, OH, United States.
E-mail addresses: komurov@hotmail.com, kkomurov@championsoncology.com (K. Komurov), Lisa.Privette@cchmc.org (L.M. Privette Vinnedge).
[1] Present address: Champions Oncology, Hackensack, NJ 07601

https://doi.org/10.1016/j.tranon.2021.101323
Received 3 September 2021; Received in revised form 12 November 2021; Accepted 19 December 2021

tumorigenesis, this system is often overwhelmed by high levels of insoluble protein species, leading to increased cell dependency on autophagy (autophagy addiction) [9]. Subsequently, autophagy inhibition may maximize the proteotoxic burden eliciting a synthetic lethality that can be exploited for therapeutic purposes.

Recently, we have described a novel molecular subtype of cancers based on the presence of abnormally high levels of transcriptional defects called TE^{def} (Transcription Elongation Defects). TE^{def} cancers are characterized by high levels of spurious transcripts, intron retention, and loss of gene body exon expression, which is observed in approximately 20% of primary breast cancers [10]. Cells with proficient transcription elongation we refer to as TE^{prof}.

In this work, we initially analyzed RNA-sequencing data from the TCGA dataset and discovered that TE^{def} tumors have extensive overexpression of the cytoplasmic protein homeostasis machinery, including several components required for autophagy. Given the fact that TE^{def} tumors produce an excessive amount of abnormal mRNA transcripts [10], we hypothesized that TE^{def} cells may produce high levels of misfolded proteins, which may lead to increased dependency on cellular protein quality control. Next, we experimentally show that TE^{def} cancer cell lines have a profound accumulation of protein aggregates (aggresomes) that appear to be associated with autophagy for clearance. We also show evidence that TE^{def} cells are more sensitive than TE^{prof} cells to autophagy inhibition *in vitro* and *in vivo*. Mechanistically, we propose that blocking the autophagy pathway maximizes proteotoxic stress, due to the accumulation of toxic protein aggregates derived from spurious defective transcripts, leading to a strong synthetic lethality in TE^{def} cells. Therefore, autophagy inhibition may be a potent treatment strategy for TE^{def} tumors, which are inherently resistant to current immunotherapies.

Materials and methods

Datasets

Processed RNA-Seq and RPPA data from The Cancer Genome Atlas (TCGA) were downloaded from the GDAC Firehose (https://gdac.broadinstitute.org/). Gene information used in the analyses, including genomic/mRNA length and Gene Ontology annotations, were downloaded from Ensembl Biomart (https://m.ensembl.org/info/data/biomart/index.html). The analyses of TCGA datasets were described in detail in [10]. NetWalker (Komurov et al.) was used for the gene network visualizations presented in the paper [11].

Antibodies and chemicals

A list of antibodies used in this study is presented in Supplementary Table 1. Chemicals were purchased from the following providers: Chloroquine diphosphate salt (CQ) (Sigma-Aldrich, St. Louis, MO, US, C6628), Hydroxychloroquine sulfate (HCQ) (Acros Organics, Carlsbad, CA, US, 263,010,250), Bafilomycin A1 (BFA) (Sigma-Aldrich, St. Louis, MO, US, SML1661), Bortezomib (Brzb) (Sigma-Aldrich, St. Louis, MO), US, 5.04314), Aphidicolin (Aph) (Sigma-Aldrich, St. Louis, MO, US, A0781), Nocodazole (Noco) (Calbiochem, San Diego, CA, US, 487,928), Flavopiridol (Flavo) (Selleckchem. Houston, TX, US, S1230), Cyclohexamide (CHX) (Sigma-Aldrich, St. Louis, MO, US, C4859), Matrigel (Corning, Corning, NY, US, 354,230) Fetal Bovine Serum (FBS) (Gibco, Waltham, MA, US, 10,437,028), Antibiotic-antimycotic (AA) (Gibco, Waltham, MA, US, 15,240,062), Leibovitz's L-15 medium (L15) (Gibco, Waltham, MA, US, 11,415,064), recombinant human Epidermal Growth Factor (hEGF) (PeproTech, Cranbury, NJ, US, AF-100–15), Insulin (Sigma-Aldrich, St. Louis, MO, US, 10,516), Glutathione reduced (Sigma-Aldrich, St. Louis, MO, US, G6013), Dulbecco's Modified Eagle Medium (DMEM) (Gibco, Waltham, MA, US, 11,965,092), Roswell Park Memorial Institute 1640 Medium (RPMI-1640) (Gibco, Waltham, MA, US, 11,875,093), Improved Minimum Essential Medium (IMEM) (Gibco, Waltham, MA, US, A1048901), Radio-Immunoprecipitation Assay (RIPA) buffer (Santa Cruz Biotechnology, Dallas, TX, US, sc-24,948).

Cell culture

Two human breast cancer cell lines with transcription elongation defects (TE^{def}), UACC-812 (CRL-1897) and MDA-MB-415 (HTB-128), were purchased from American Type Culture Collection (ATCC, Manassas, VA, US). UACC-812 cells were cultured in Leibovitz's L-15 medium with 2 mM L-glutamine supplemented with 20 ng/ml hEGF, 20% FBS, and 1% AA. MDA-MB-415 cells were cultured in L-15 medium with 2 mM L-glutamine supplemented with 10 μg/ml insulin, 10 μg/ml glutathione reduced, 15% FBS and 1% AA. For all laboratory assays, the L-15 base medium was replaced with DMEM supplemented with all the components mentioned above. Four transcription elongation proficient (TE^{prof}) human breast cancer cell lines SKBR3 (HTB-30), CAL51 (ACC-302), T47D (HTB-133), and MDA-MB-453 (HTB-131) were originally obtained from ATCC (Manassas, VA, US) or the Leibniz Institute (DSMZ, Braunschweig, Germany). SKBR3, CAL51, and T47D cells were cultured in RPMI-1640 supplemented with 10% FBS and 1% AA. MDA-MB-453 cells were cultured in Improved IMEM containing 20% FBS with 1% AA. B16/F10 mouse melanoma cell line was obtained from ATCC (Manassas, VA, US) and cultured in DMEM supplemented with 10% FBS and 1% AA. To synthetically create a TE^{def}-like signature, B16/F10 cells were treated with a sub-lethal dose (25 nM) of Flavopiridol ("Flavo") for 6 days prior to analysis, replenishing every three days. All cell lines were cultured at 37 °C in a humidified atmosphere with 5% CO_2, except the UACC-812 and MDA-MB-415 cells grown in L-15 base medium, which were cultured in 0% CO_2.

Lentiviral transduction of shRNA

HEK293T cells were obtained from ATCC (Manassas, VA, US) and cultured in DMEM supplemented with 10% FBS and 1% AA. Lentiviral vectors were produced by co-transfection of HEK293T cells with lentiviral packaging plasmids (VSV-G and delta 8.9) and ATG5-shRNA expressing plasmid (Sigma-Aldrich, St. Louis, MO, US, TRCN0000151963) using jetPRIME transfection reagent (Polyplus Transfection, Illkirch, France, 114–15). Viral supernatant was collected for three days, filtered, and concentrated by ultracentrifugation at 25,000 rpm for 2 h at 4 °C. B16/F10 cells were seeded in 6-well plates at low density (8×10^3 cells/well) and pre-treated with 25 nM Flavo (added to the cell suspension at seeding time) for 3days. After three days, both untreated and Flavo-pretreated cells were transduced overnight with the concentrated viral supernatant (25 μl/well) in the presence of 8 μg/ml polybrene then incubated in fresh medium for an additional 48 h. 25 nM Flavo treatment was maintained throughout transduction.

Immunoblotting assays

Western blotting (WB)

Cells were grown to 70–80% confluency and directly lysed with RIPA buffer. Lysates were cleared by centrifugation (14,000 rpm, 10mins, at 4 °C) and quantified by DC Protein Assay Kit (Bio-Rad, Hercules, CA, US, 5,000,111) using the manufacturer's microplate assay protocol. Generally, 15–30 μg protein was resolved in 4–15% Precast Protein Gels (Bio-Rad, Hercules, CA, US, 4,561,086), and transferred onto nitrocellulose membranes. The membranes were blocked with 5% dry milk in Tris-Buffered Saline-Tween-20 (TBS-T) for 1hr then incubated overnight with primary antibodies (Supplementary Table 1) in 5% bovine serum albumin in TBS-T. After washing and incubating with the appropriate secondary antibody, protein signals were detected with Immobilon Western Chemiluminescent Horseradish Peroxidase (HRP) Substrate Kit (Millipore, Burlington, MA, US, WBKLS0500) using Azure C500 imaging system (Azure Biosystems, Dublin, CA, US). Signal intensities of select

proteins were quantified by densitometry using ImageJ software (National Institutes of Health, Bethesda, MD, US).

Soluble/insoluble fractionation

Soluble and insoluble fractions of cell lysates were prepared as previously described [12]. Briefly, cells were washed, scraped into 1 ml ice-cold phosphate-buffered saline (PBS), and pelleted by centrifugation (100× g, 5mins, 4 °C). Cell pellets were re-suspended in 300µl lysis buffer containing 20 mM Tris–HCl pH7.5, 150 mM NaCl, 1.2% deoxycholate, 1.2% Triton X-100, 200 mM iodoacetamide (Sigma-Aldrich, St. Louis, MO, US, I6125), and 1X Halt EDTA-free protease inhibitor cocktails (ThermoFisher Scientific, Waltham, MA, US, 78,430). Iodoacetamide and protease inhibitor cocktails were added to the lysis buffer just before use. Samples were sonicated (5×, 30s at 30% amplitude with 30s intervals) and the insoluble proteins were isolated upon centrifugation at 16,200× g for 30mins at 4 °C. Supernatants (soluble fractions) were washed 3X with lysis buffer before being solubilized in 2% SDS. Both soluble and insoluble lysates were quantified and immunoblotted as mentioned in the WB section. The soluble fraction prepared according to this protocol acquired a strong acidic pH due to the high concentration of Iodoacetamide and was neutralized with a few drops of 1 M Tris–HCl, pH8.0.

Native gel analysis

Native lysate preparation protocol was adapted from previously described protocols [13–15]. Briefly, cells were collected from at least two 10 cm plates (70–80% confluent), scraped into 1.5 ml ice-cold PBS, and pelleted at 100× g for 5mins at 4 °C. Cell pellets were re-suspended in 200µl/plate lysis buffer (50 mM Tris–HCl, pH8, 5 mM MgCl2, 0.5 mM EDTA, 2 mM ATP, 0.2% Nonidet P-40 (NP-40), 1X Halt EDTA-free protease inhibitor cocktail (ThermoFisher Scientific, Waltham, MA, US, 78,430). ATP and protease inhibitor cocktails were added to the lysis buffer just before use. Cell suspensions were subjected to 30 strokes within 30 s on ice in a Dounce homogenizer and incubated on ice for 5–10mins without vortexing. Extracts were clarified by centrifugation (14,000 rpm, 30mins, 4 °C) and supernatants (native lysates) were quantified as mentioned in the WB section. Protein samples prepared and processed as follows. Lysates were mixed with 2× native sample buffer (Bio-Rad, Hercules, CA, US, 1,610,738) at 1:1 ratio and quickly loaded into 3–8% Criterion™ XT Tris-Acetate Precast Gels with no SDS (Bio-Rad, Hercules, CA, US, 3,450,129). Gels were ran in 1X SDS-free Tris/Glycine Buffer (Bio-Rad, Hercules, CA, US, 1,610,771) for 1hr at room temperature (RT) using a low voltage (50 V), followed by 3–4 h at 4 °C using a high voltage (150 V). Gels were ultimately transferred onto nitrocellulose membranes and immunoblotted as described in the WB section.

Immunofluorescent assays

Human breast cancer cell lines (TE^{prof}/TE^{def} phenotype) were seeded in 8-well chambered coverslips (ibidi, Gräfelfing, Germany, 80,826) at a density of $5–10\times10^4$ cells/well and incubated 24–72 h to obtain desired cell densities. B16/F10 cells (synthetic TE^{prof}/TE^{def} model) were also seeded (with or without 25 nM Flavo) in 8-well chambered coverslips at low density (750 cells/well) and grown for 6 days. Cells were fixed in 3.7% formaldehyde diluted in PBS and permeabilized in 0.25% Triton *X* − 100 in PBS. Permeabilized cells were blocked in 10% normal goat serum (Cell Signaling, Danvers, MA, US, 5425) diluted in the permeabilization solution for 1hr at RT. Primary antibodies (Supplementary Table 1) or Proteostat reagent (described below) were used to stain the cells.

For detection of autophagy, cells were incubated overnight at 4 °C with antibodies specific to the autophagy detection markers microtubule-associated protein 1 light chain 3 beta (LC3B) (D11) (1:200), and autophagy related 16 like 1 (pATG16L1) (1:150) in human cell lines, and LC3B (G-9) (1:200) in mouse cells. The LC3B and pATG16L1 puncta volume and/or signal intensity were used to determine autophagy status in different cell lines or conditions. Alexa Fluor-conjugated secondary antibodies (Supplementary Table1) diluted in permeabilization solution (1:1000) were used to detect primary antibodies (1hr at RT) and Hoechst-33,342 reagent diluted in PBS (1:1000) was used for nuclear staining.

Aggresomes and misfolded proteins were observed with Proteostat Aggresome Detection Kit (Enzo Life Sciences, Farmingdale, NY, US, ENZ-51,035-K100) following the provider's instruction. Cells were stained with a dual detection reagent containing Hoechst-33,342 (1:1000) and Proteostat reagent (1:5000). After removing the excess staining solution and washing twice with PBS, the stained cells were kept in PBS and analyzed for aggresome puncta and nuclear signal using a customized excitation/emission setting (488/620) of a Nikon Confocal Microscope described below.

Stained cells (antibody or Proteostat stained) were visualized with a Nikon A1R LUN-V confocal scanner on a TiE inverted Microscope (Nikon Instruments, Tokyo, Japan) using 60X PlanApo IR NA 1.27- Water Immersion and 100X Apo TIRF NA 1.49- Oil Immersion lenses at appropriate excitation/emission wavelengths for each fluorophore and/or dye. Z-stack three-dimensional (3D) images were taken when required and used for image quantification with Bitplane Imaris software v9.5.1 (Oxford Instruments, Abingdon, United Kingdom).

Image quantification in Imaris

2D or 3D Z-stack images were used to quantify signal intensity or puncta volume per cell, respectively, following the Imaris Reference Manual. Briefly, Z-stack images were opened into a multi-channel 3D model with no pre-processing. To designate individual puncta of interest, the Surface creation wizard was applied to generate a region of interest (ROI) using an appropriate source channel. The auto-threshold and background subtraction features of the software were used to separate the ROIs. The total number of cells in each filed was determined based on the nuclear stain using the auto-threshold and background subtraction features. The total volume of the ROIs in each field was normalized to the total number cells to calculate the volume of ROI per cell in µmˆ3. The signal intensity of the ROI was calculated in the same way.

Flow cytometry analysis

Human breast cancer cell lines (TE^{prof}/TE^{def} phenotype) were seeded in 6-well plates ($2–5\times10^5$ cells/well) and grown overnight. B16/F10 cells (synthetic TE^{prof}/TE^{def} model) were seeded in 6-well plates at low density (8×10^3 cells/well) and grown for 6 days with or without 25 nM Flavo. Cells were harvested by trypsinization and cell pellets ($\sim1\times10^6$ cells) were washed twice in PBS and fixed with 1 ml of 3.7% formaldehyde in PBS then permeabilized with 0.5% Triton X-100 in PBS. Cells were washed in PBS and used for different assays (as detailed below) and the data were analyzed using a FACSCanto flow cytometer and FACS-Diva software (BD Biosciences, Franklin Lakes, NJ, US).

Aggresome detection assay by flow cytometry

This assay was performed using Proteostat Aggresome Detection Kit (see above) following the provider's instruction. Briefly, permeabilized cells were re-suspended in 500 µl Proteostat reagent (1:25,000) and incubated for 30mins at RT protected from light. After removing the excess staining solution and washing once with PBS (800x g, 15mins, RT), the stained cells were re-suspended in 300–500 µl PBS and analyzed by flow cytometry. The aggresome signal (median fluorescent intensity) was detected through a customized channel where the excitation/emission was set to 488/610–20 nm.

Protein synthesis rate assay

Newly synthesized (nascent) proteins were detected with the Click-iT HPG Alexa Fluor Protein Synthesis Assay Kit (ThermoFisher Scientific,

Waltham, MA, US, C10428) following the manufacturer's protocol with slight modification. Briefly, cells were seeded as described above and cell culture medium was replaced with 1 ml methionine-free medium containing 50 μM L-homopropargylglycine (HPG) and incubated at 37 °C for 1hr. The HPG labelled cells were washed with PBS and harvested by trypsinization. Cell pellets (~1 × 10^6 cells) were fixed and permeabilized then re-suspended in 500μl freshly prepared click-iT reaction cocktail and incubated for 30mins at RT in the dark. The click-iT reaction cocktail was prepared according to the provider's protocol with the exception of a 10-fold reduction in the amount of Alexa Fluor 488 azide reagent. When co-staining, Alexa Fluor 647 azide was used to detect the HPG labelled-nascent proteins first then counterstained with the Proteostat reagent. Cells were analyzed by flow cytometry and the median fluorescent intensity of the cells was determined using the appropriate channels of the flow cytometer.

Viability using Propidium Iodide (PI)

This assay was performed using Propidium Iodide/RNase Staining Buffer (PI) (BD Biosciences, Franklin Lakes, NY, US, 550,825) as previously described [16]. Briefly, cells were seeded as described above and drug treated for three days. Cells were harvested by trypsinization, washed with PBS, and re-suspended in 500μl PI/RNase staining buffer (BD Biosciences, Franklin Lakes, NY, USA #550,825) per 1 × 10^6 cells for 15mins. Percentage of live/dead cells were determined within 1hr after staining by flow cytometry using the standard PI channel (excitation/emission 561/600 nm) of a BD FACSCanto cytometer (BD Biosciences). For each sample, 50,000 events were collected in duplicate.

Two-dimensional (2D) cell culture cytotoxicity assay

This assay was performed using CellTox Green Cytotoxicity Kit (Promega, Madison, WI, US, G8731) following the manufacturer's instruction. Briefly, human breast cancer cells were seeded in black 96-well clear bottom assay plates (Corning, Corning, NY, US, 3603) (5–10×10^3 cells/well in 50 μl medium) and recovered overnight. Cells were co-treated with CQ (10, 25, 50, 100, and 250 μM) and 1X CellTox Green reagent and incubated for 72 h at 37 °C. The fluorescent signal was captured with a FlexStation3 Multi-Mode Microplate Reader (Molecular Devices, San Jose, CA, US) at excitation/emission 500/530 nm.

Three-dimensional (3D) spheroid cultures and viability analysis

This assay was performed using CellTiter-Glo 3D Cell Viability Kit (Promega, Madison, WI, US, G9682) following the manufacturer's instruction. Briefly, B16/F10 cells were seeded in Ultra-low attachment round bottom 96-well plates (Corning, Corning, NY, US, 7007) at a concentration of 200 cells/well in 200ul growth medium (DMEM with 10%FBS and 1%AA). Half of the plate was left untreated (control) and the other half was treated with 25 nM Flavo added to the cell suspension at the time of seeding. Cells were incubated for three days at 37ºC. After confirming spheroid formation (one spheroid/well) under a bright field microscope, 100ul of the culture medium was carefully removed and replaced with 100ul fresh medium containing CQ (2.5, 5, 10, and 15 μM), BFA (2.5, 5, 7.5, and 10 nM), or Brzb (10, 25, 50, 100 nM) and incubated for an additional three days. 25 nM Flavo exposure was maintained through day 6. To test viability, 100ul of the culture medium was replaced with 100ul of the CellTiter-Glo 3D Reagent, shaken vigorously for 5mins, and incubated for an additional 25mins at RT. The luminescent signal of the spheroids was captured with a FlexStation3 Microplate Reader. Each cell line was tested for sphere-forming ability, but only B16 cells were capable of forming spheroids in culture.

Proteasome activity assay

Proteasome activity was assessed using a fluorometric assay kit from Abcam (Waltham, MA, US, ab107921). Briefly, 2 × 10^6 cells were harvested by trypsinization, washed with cold PBS, and lysed in 60 μl 0.5% NP-40 (Sigma-Aldrich, St. Louis, MO, US, NP40S). Lysates were clarified by centrifugation at 13,000 rpm for 12mins at 4 °C then supernatants were separated and diluted 1:3 with the assay buffer. Samples were transferred into 96-well black assay plates and assayed per the manufacturer's instruction. The fluorescent signal was captured at different time intervals using a FlexStation3 Microplate Reader with excitation/emission wavelengths set to 350/440 nm.

Real-time quantitative polymerase chain reaction (RT-qPCR)

Total RNA was extracted from cultured cells using RNeasy Mini Kit (Qiagen, Hilden, Germany, 74,134). Reverse transcription was carried out using SuperScript first strand kit (Invitrogen, Waltham, MA, US, 11,904,018). Gene expression was measured using GoTaq qPCR Master Mix (Promega, Madison, WI, US, A6001) and the Applied Biosystems Real-Time PCR machine (Life Technologies, Waltham, MA, US). Gene expression was normalized to glyceraldehyde-3-phosphate dehydrogenase (GAPDH). ATG5 knockdown was confirmed by RT-PCR using specific primers (F_5`−3`: ATGGACAGCTGCACACACTT, R_5`−3`: AGAGGGGTTTCCAGCATTGG).

Soluble/Insoluble RNA extraction and sequencing

Soluble/Insoluble RNA extracts were prepared as previously described [17]. Briefly, cells were scraped into 1.5 ml ice-cold buffer containing 50 mM Tris pH 7.6, 50 mM NaCl, 5 mM MgCl2, 0.1% NP-40, 1 mM β-mercaptoethanol, 1X Halt EDTA-free protease inhibitor cocktails (ThermoFisher Scientific, Waltham, MA, US, 78,430), and 0.4 U/ml SUPERase•In RNase inhibitor (Invitrogen, Waltham, MA, US, AM2696) on ice. Cell suspensions were subjected to 30 strokes within 30 s in a Dounce homogenizer on ice, followed by centrifugation at 2000× g for 2mins at 4ºC. 125 μl of the supernatant was mixed with 375 μl Trizol (Invitrogen, Waltham, MA, US, 15,596,018) to isolate the total cytosolic RNA and the remainder (~1 ml) was centrifuged at 10,000× g for 10mins at 4ºC to separate the soluble fraction from the insoluble fraction (pellet). The insoluble pellet was re-suspended in 500 μl Trizol to isolate the insoluble cytosolic RNA. Trizol RNA extraction was performed using Direct-zol RNA miniprep (Zymo Research, Irvine, CA, US, R2050) following the manufacturer's protocol. The extracted RNA samples (total cytosolic and insoluble cytosolic RNAs) were used for Poly A RNA sequencing at the University of Cincinnati Sequencing Core (Cincinnati, OH, US). Differentially expressed genes (+1.25/−1.25 fold change cutoffs) for each fraction were pooled for TE^{def} and TE^{prof} cell lines then analyzed for significant gene ontologies using GO-Elite. Gene network maps were created with Cytoscape and Netwalker [11].

In vivo tumorigenesis

Eight-week-old female C57BL/6 mice were purchased from Jackson Laboratory (Bar Harbor, ME, US) and acclimated for 1–2 weeks. Mice were randomized into two groups and the injection sites were shaved to facilitate cell injection and tumor measurement. Freshly prepared suspensions of 5 × 10^5 cells in 200 μl PBS/Matrigel (1:1 ratio) were injected subcutaneously into the right flank of the mice. One group was injected with untreated B16/F10 cells (control, $n = 8$) and the other group with Flavopiridol pretreated (25 nM, 6 days) cells (Flavo, $n = 8$). Tumors were grown until palpable (~8–10 days) before animals in each group were randomized into two sub-groups; PBS and hydroxychloroquine (HCQ). Mice in each sub-group were injected intraperitoneally (IP) with 100 μl PBS ($n = 4$) or HCQ (60 mg/kg/day, $n = 4$). IP injections were carried out 5 days per week for three weeks. Tumors were measured three times a week using digital calipers. Mouse body weight, one of the parameters for evaluating the systemic toxicity of HCQ treatment, was also measured three times per week. Tumor volume was calculated using a previously described formula $[(\pi/6)\times L \times W\hat{}2]$ [18,19]. Usage and

handling of mice was performed with the approval of the Cincinnati Children's Institutional Animal Care and Use Committee under protocol 2017–0061. All mice were housed in specific pathogen free housing with ad libitum access to food and water.

Statistical analysis

Unpaired two-tailed Student's *t*-test was used to determine the level of significance and the error bars represent standard error of data

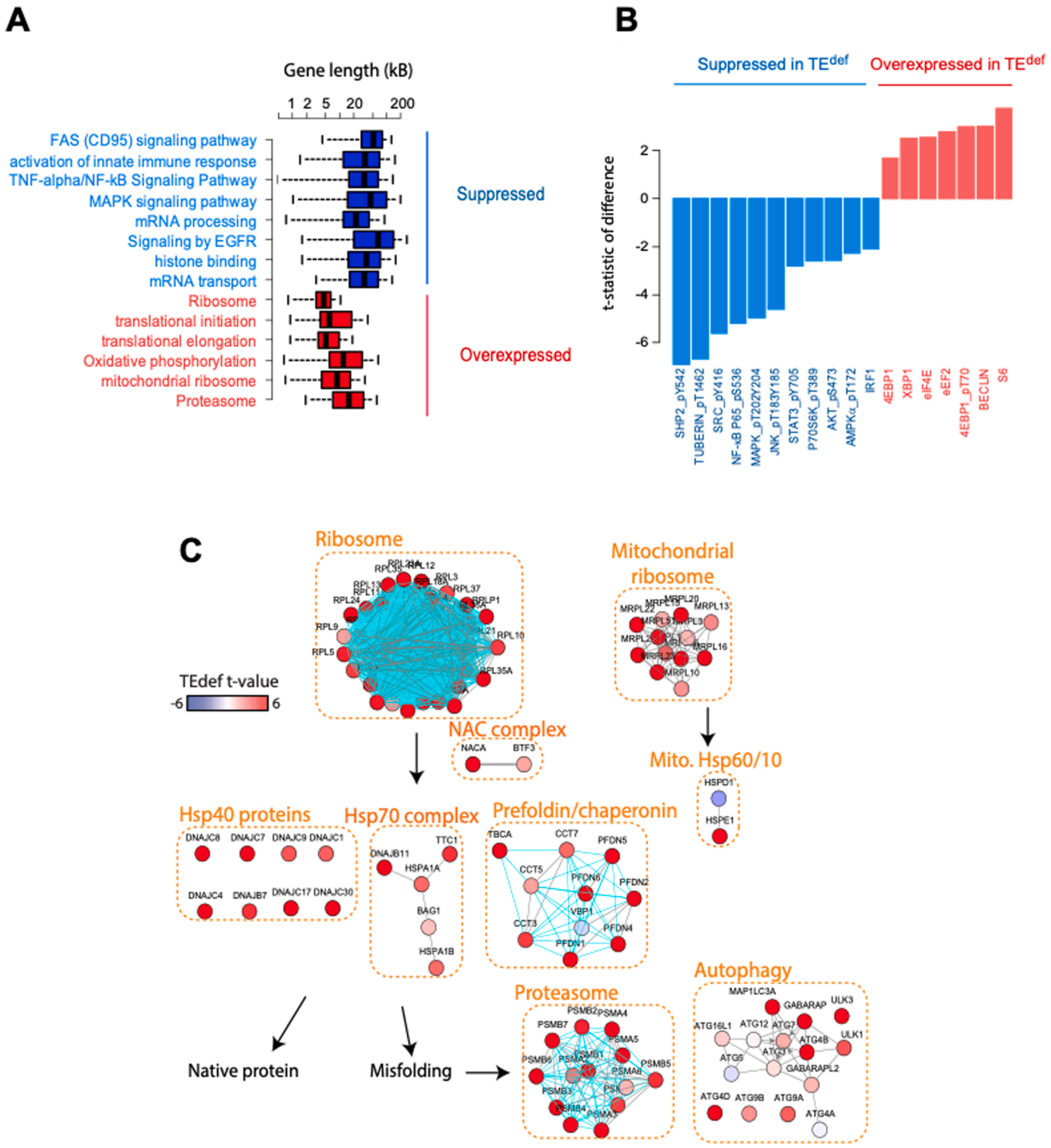

Fig. 1. Protein homeostasis pathways are overexpressed in TEdef cancers: A. Gene length distribution of genes within the indicated pathways that are either significantly suppressed (blue) or overexpressed (red) at the mRNA level in TE^{def} cancers in TCGA datasets; **B.** Bar plot of the t-statistic of difference of the expression of selected protein markers in TE^{def} vs TE^{prof} cancers in TCGA datasets, based on the reverse-phase protein array (RPPA) data. A t-statistic of |1.98| corresponds to a p-value of 0.05, with the sign of the t-statistic indicating the direction of difference. **C.** A network view of the protein homeostasis pathways that are significantly overexpressed in TE^{def} cancers in TCGA datasets. The coloring of nodes reflects the t-statistic of correlation of the mRNA expression values of corresponding genes with TE^{def} (higher value reflects higher expression in TE^{def} and vice versa).

collected from at least three independent experiments unless otherwise mentioned. Asterisks denote the level of significance where one asterisk (*) indicates $p<0.05$, two asterisks (**) indicates $p<0.01$, three asterisks (***) indicates $p<0.001$, and "ns" indicates non-significant differences. Both error bars and p values were calculated using Prism software (GraphPad, San Diego, CA, US).

Results

TE^{def} tumors upregulate genes involved in protein homeostasis and quality control

Gene expression profiles of TE^{def} tumors were analyzed to identify potential mechanisms that permit their survival despite the presence of excessive levels of aberrant mRNA transcripts. We identified a significant upregulation of genes that code for proteins that function in various stages of protein synthesis and folding, including translational initiation and elongation (Fig. 1A). Upon further examination, we determined that TE^{def} tumors also over-express genes that code for proteins in the proteasome and autophagy pathways (Fig. 1B). Furthermore, while gene ontology analysis identified immune system genes to be repressed, as previously published [10], genes involved in the proteostasis network were over-expressed (Fig. 1A,C). Thus, we hypothesized that TE^{def} tumors may upregulate the protein quality control pathways to circumvent the proteotoxic stress exerted by the defective transcripts.

TE^{def} cells contain high levels of insoluble ubiquitinated protein aggregates

To further elucidate the consequences of defective transcription elongation, we utilized cell lines we previously identified to be TE^{def}, based on RNA-Seq data in the Cancer Cell Line Encyclopedia [10]. Only four available cell lines demonstrate a TE^{def} phenotype, two of which are breast cancer in origin. We therefore compared these two TE^{def} breast cancer cell lines with three breast cancer cell lines that are TE^{prof}. We chose cell lines that represent the three major molecular subtypes of breast cancer, triple negative (CAL51), estrogen receptor alpha positive (T47D) and HER2+ (SKBR3). Truncated and defective transcripts are often correlated with protein misfolding, aggregation, and aggresome formation [2,20,21]. In line with this notion, we observed a higher level of aggresomes in the TE^{def} cell lines versus TE^{prof} (i.e. cancer cell lines that do not have TE defects) cell lines using the Proteostat reagent, which fluorescently labels protein aggregates (Fig. 2A,B; $p = 0.001$). The protein aggregates were clustered into distinct aggresome puncta throughout the cytoplasm supporting the notion that the TE^{def} cells suffer from a profound proteotoxic burden exerted by their defective transcription signature.

Realizing the limitation of using two genetically distinct TE^{def} cell lines, we chose to complement these findings with an isogenic model. We used a small molecule inhibitor approach to phenocopy the TE^{def} profile by treating B16 mouse melanoma cells with flavopiridol ("Flavo"), a CDK9 kinase inhibitor that blocks transcription elongation as used previously to model the TE^{def} phenotype [10]. Using confocal imaging, we observed a significant increase ($p = 0.005$) in Proteostat labeled protein aggregates in the Flavo treated cells (Sup. Fig. 1A,B). We then co-labeled protein aggregates and nascent proteins and analyzed the cells using flow cytometry. As expected, the aggresome level was markedly increased ($p = 0.0003$) in the Flavo treated cells despite a substantial reduction ($p = 0.0001$) in the global protein synthesis. The ratio of protein aggregates to nascent protein synthesis indicates that TE^{def} cells experience a significant ($p = 0.003$) proteotoxic burden (Sup. Fig. 1C–E).

Protein aggregates that result from sequestered terminally misfolded gene products are usually insoluble. In line with this notion, our western blot for soluble/insoluble fractionated lysates, showed a significant amount ($p = 0.006$) of insoluble poly-ubiquitinated proteins (poly-Ub) accumulated in the TE^{def}, but not TE^{prof} lysates, while no difference for the soluble poly-Ub proteins was detected (Fig. 2C,D). To further characterize the composition of the insoluble fraction, we compared the RNA in the soluble and insoluble fractions from TE^{prof} and TE^{def} cells. The insoluble fraction of TE^{def} cells consisted of more mRNA transcripts, from a larger number of genes, compared to TE^{prof} cells (Fig. 2E, F). A gene ontology analysis of transcripts enriched in the insoluble fraction of TE^{def} cells (Fig. 2G) identified many of the same, or highly similar, gene ontologies of suppressed genes in TE^{def} cells in TCGA datasets shown in Fig. 1A. Gene network analysis of enriched genes in the insoluble fraction using Cytoscape are shown in Sup. Fig. 2. Combined, this suggests that mRNAs most impacted by transcription elongation defects are absent from standard RNA-Seq preparations of soluble mRNA and are, instead, trapped within insoluble complexes.

Increased poly-Ub proteins in the insoluble fraction indicates that clearance of these proteins through the unfolded protein response (UPS) is defective, leading to their aggregation. Increased mRNA in the insoluble fraction indicates that ribosomal complexes (possibly stalled) are incorporated into insoluble stress granules. Combined, this data led us to explore the status of the protein quality control machinery in TE^{def} versus TE^{prof} cells in more detail.

The proteasome system is compromised in TE^{def} cells

Protein synthesis and folding is tightly regulated by the components of the proteostasis network to ensure that the terminally misfolded proteins are eliminated [1,22]. We analyzed the expression of several key components of the proteostasis network including p97/VCP, HSP70, HSPA5/BiP, TIAR, and Ubiquitin. Surprisingly, we did not observe changes in expression levels of these proteins in the TE^{def} cells. A slight increase (non-significant) in the level of stress response molecules such as HSP70 and TIAR (a stress-granule marker) was detected in the TE^{def} cells (Fig. 3A). This response does not seem to activate the endoplasmic-reticulum-associated protein degradation (ERAD) pathway, as levels of the binding immunoglobulin protein (BiP or HSPA5) and p97/VCP were not significantly changed (Fig. 3A). This finding indicates that the classical unfolded protein response is likely not triggered in these cells, perhaps due to some defect in signaling or transcription related to TE^{def}.

The proteasome complex consists of a 20S proteolytic core particle and a 19S regulatory particle. The 19S regulatory subunit is thought to govern the recognition and entry of the ubiquitinated substrates into the interior of the 20S core particle for degradation [5,23]. To check the functionality of the proteasome complex, we first analyzed the TCGA datasets for differentially expressed genes in TE^{def} vs TE^{prof} tumors and found that the expression of many genes of the 19S regulatory particle of the proteasome complex were downregulated, while those of the 20S core particle were upregulated in TE^{def} tumors (Fig. 3B). These data suggest that the proteasome system might be compromised, encouraging us to further investigate the expression of the 19S regulatory subunit in the TE^{def} vs TE^{prof} cells.

Interestingly, our standard western blot analyses showed that the protein expression of essential components of the 19S particle, such as PSMD2, was significantly reduced ($P = 0.004$) in the TE^{def} cells and the expression of other 19S subunits, such as PSMD1 and PSMD11, were also reduced but not to a significant level. However, the expression ($p = 0.012$) and catalytic activity of the core subunit (20S α&β) of the proteosome was increased in both human TE^{def} cells and the B16 phenocopy model (Fig. 3C–E and Sup. Fig. 3A, C,D). This change in protein expression seems to be specific to the proteasomal regulatory subunit as the expression of ribosomal markers such as RPS3 and RPL5 remained unchanged (Fig. 3C). Furthermore, native gel western blot analysis showed that the level of both capped 26S proteasome and the free 19S sub-complexes were reduced ($p = 0.020$) in the TE^{def} cells (Fig. 3F,G and Sup. Fig. 3B). These data suggest that, although the 20S catalytic activity is enhanced, the degradation capacity of the proteasome system is likely compromised in the TE^{def} cells due to suppression of essential 19S

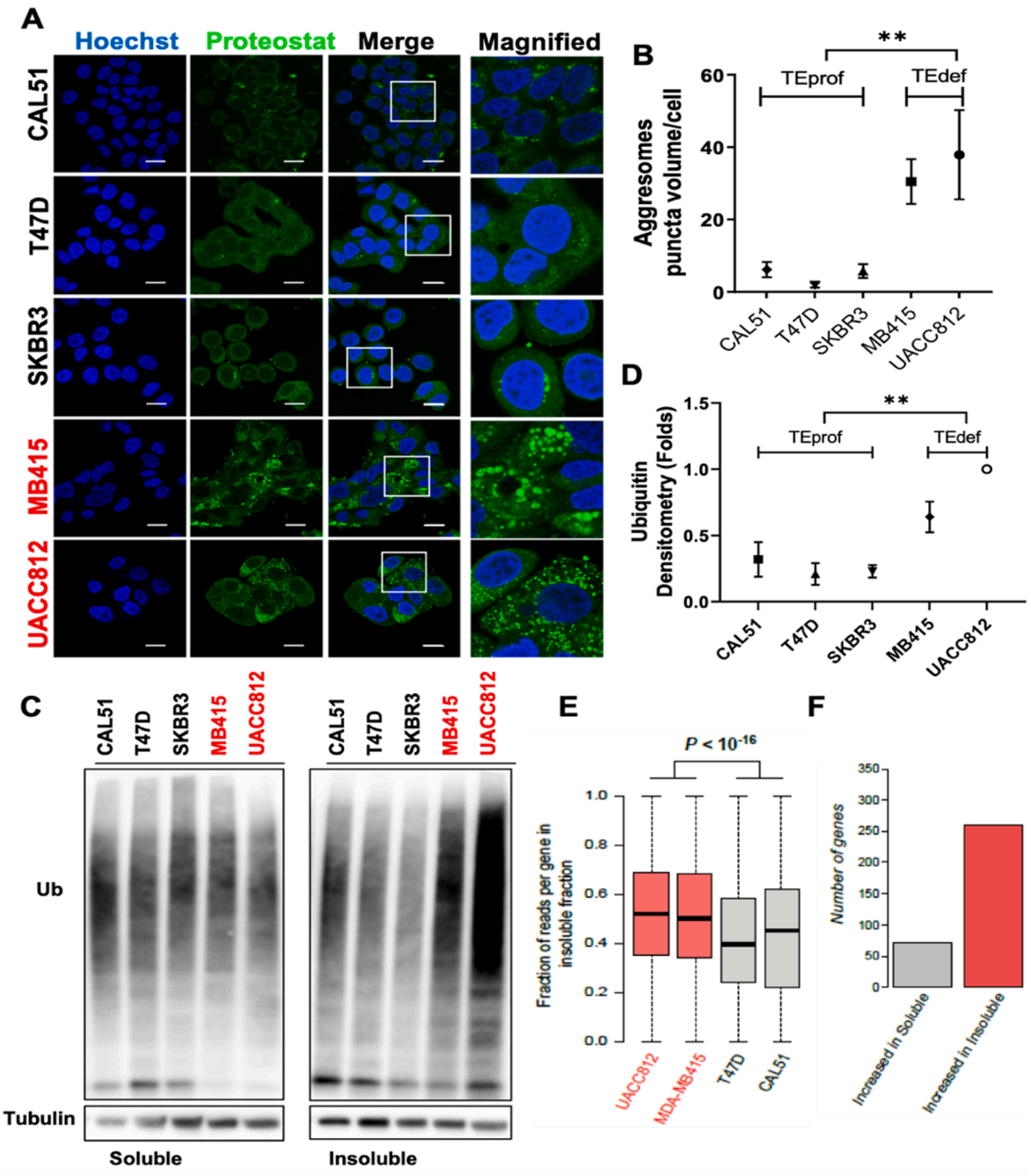

(caption on next page)

Fig. 2. TE^{def} cells contain high levels of insoluble protein aggregates (aggresomes): A. Confocal images show aggresome puncta in control (black) versus transcriptionally defective (red) breast cancer cell lines stained with Proteostat reagent as indicated. The right panel represents magnified views of the white boxed regions, scale bars; 20 μm; **B.** Quantification of aggresome puncta volume calculated from 3D Z-stack confocal images in **A**, mean values of two independent experiments are shown; **C.** Immunoblots show insoluble ubiquitinated protein aggregates in the insoluble fraction of the TE^{def} lysates; **D.** Densitometry quantification of the ubiquitinated protein aggregates in the insoluble fraction of **C** with fold changes normalized to UACC812; **E.** For each gene, the reads in the soluble and the insoluble fractions were pooled per cell line, and the proportion of reads in the insoluble fraction over total was calculated (0 meaning all the reads for that gene came from the soluble fraction, and 1 meaning that all the reads for that gene came from the insoluble fraction). The boxplot here shows the distribution of these proportions for all the genes in each sample, showing a significant enrichment in the TE^{def} cells. **F.** For each gene, differential expression using *t*-test was calculated between TE^{def} and TE^{prof} cells in the soluble and insoluble fractions. The barplot shows the number of genes that were found to be significantly ($P < 0.05$) increased in TE^{def} cells in the soluble and insoluble fractions. More genes were found increased in the insoluble fraction in TE^{def} cells **G.** GO-Elite was used to analyze the gene ontologies of differentially expressed genes that were enriched in the insoluble fraction of TE^{def} cell lines compared to TE^{prof} cell lines. **=p<0.01.

regulatory components. To further test the function of the proteasome system, we performed a brief 3-hour treatment of TE^{prof} and TE^{def} cells with the proteasome inhibitor bortezomib. Interestingly, TE^{prof} cells respond to this inhibition with an expected increase in total ubiquitination of proteins by western blotting. However, TE^{def} cells do not respond and show less ubiquitination, indicating that the proteasome may be malfunctioning and ubiquitinated proteins are being removed by another mechanism (Sup Fig. 4).

TE^{def} cells upregulate markers of autophagy induction

Toxic protein aggregates are often degraded through the autophagy pathway [24]. Using immunofluorescence and confocal microscopy, we observed a strong induction of autophagy in the TE^{def} cells, indicated by higher levels ($p = 0.0003$) of the core autophagy marker LC3BII (Fig. 4A, B). Autophagy flux was further confirmed via immunofluorescence by the upregulation of pATG16L1 ($p = 0.002$) using anti-pATG16L1, a monoclonal antibody that detects newly formed autophagosomes [25] (Fig. 4C, D). Autophagy upregulation in the TE^{def} cells was further confirmed by western blot analysis for LC3BII/I ($p = 0.036$) and pATG16L1 ($p = 0.007$) (Fig. 4E and Sup. Fig. 5A,B). Furthermore, sequestosome 1 (SQSTM1/p62), which binds to LC3 and is degraded when autophagy is induced, was also down-regulated. Notably, this pattern of autophagy flux was also observed in the isogenic, flavopiridol-induced TE^{def} model in which we observed a higher level of LC3B by immunofluorescence ($p = 0.0004$) and western blot ($p = 0.0004$) in the Flavo-treated B16 cells while the level of SQSTM1 (p62) was down (Sup. Fig. 5C–F).

Chloroquine (CQ) and hydroxychloroquine (HCQ) have been broadly used to inhibit autophagy for cancer treatment [26–30]. Importantly, brief (3 h) autophagy inhibition by CQ led to a significant ($p = 0.021$) accumulation of aggresomes in the TE^{def} but not TE^{prof} cells (Sup. Fig. 5 G,H). This indicates an increased dependency on the autophagy pathway in the TE^{def} cells to degrade the toxic aggresomes.

TE^{def} cells are sensitive to autophagy inhibition

Next, we explored the possibility of using autophagy inhibition as a therapeutic strategy in TE^{def} cancer cells. We first, conducted a series of viability assays in 2-dimensional (2D) adherent cell culture. Increased sensitivity to autophagy inhibition by pharmacological drugs such as chloroquine (CQ) and bafilomycin-A1 (BFA) was observed in both TE^{def} breast cancer cell lines ($p<0.007$ for CQ) (Fig. 5A and Sup. Fig. 6A) and Flavo-treated B16 cells ($p<0.0001$ for both CQ and BFA) (Fig. 5C and D, Sup Fig. 6A) compared to TE^{prof} models. Interestingly, these cells were not sensitive to proteasomal inhibition by bortezomib (Brzb) (Fig. 5B,E Sup Fig.7A) or DNA replication stress by aphidicolin (Aph) (Sup. Fig. 6B). Importantly, this pattern of sensitivity was robustly observed for both CQ ($p = 0.0015$) and BFA ($p<0.0001$) in the 3-dimensional culture of B16-Flavo spheroids (Fig. 5F–H). The TE^{def} cells (both breast cancer and Flavo-treated B16 cells) consistently showed lower IC50 to CQ and BFA in the conditions mentioned above (Fig. 5A–H).

Sensitivity to autophagy inhibition was further confirmed by a genetic approach where knocking down ATG5 (Sup. Fig. 6C), an essential gene in the autophagy pathway, showed similar effect to CQ & BFA on the viability of B16-Flavo cells (Sup. Fig. 6D). Intriguingly, the B16-ATG5-knockdown cells maintained their sensitivity to autophagy inhibition even after Flavo withdrawal for 3 and 6 days (Sup. Fig. 6E). This indicates that the effects of transcription elongation inhibition by flavopiridol may not be reversible, or at least takes a long time to recover.

We then tested the therapeutic efficacy of targeting autophagy to treat TE^{def} tumors in an immunocompetent murine model in vivo. Similar to our *in vitro* data, tumors derived from flavopiridol pretreated B16 cells (25 nM for 6 days) showed increased sensitivity to autophagy inhibition by HCQ compared to tumors from control cells while the animals demonstrated no significant changes in weight (Fig. 5I and Sup Fig. 7B). These tumors continued to show lower levels of p-Ser2 and p-Ser5 RNAPII, which are required for RNAPII elongation function [10], after four weeks of growth *in vivo* (Fig. 5J).

Overall, these data suggest that TE^{def} cells acquired an addiction to autophagy in order to maintain proteostasis and survival. Accordingly, autophagy inhibition causes a strong synthetic lethality that can be exploited for therapeutic purposes for this molecular sub-type of immunotherapy-resistant cells/tumors.

Discussion

Successful cancer therapy depends on identification of critical genes/pathways that are exploited by cancer cells. Dependency on such pathways could be related to a variety of factors involved in carcinogenesis, including both genetic (DNA mutations/aberration) and non-genetic modifications. The latter can be exemplified by epigenetic changes and transcriptional/translational errors that expose cancer cells to specific vulnerabilities due to the formation of various subsequent stress phenotypes, such as metabolic, mitotic, proteotoxic stress [10,31]. These stress phenotypes have been extensively studied over the past two decades and are now considered hallmarks of cancer [32–34]. To survive and grow, cancer cells must evolve mechanisms (stress support pathways) that enable them to buffer their stressful environment. Interventions that impair the function of these stress support pathways may cause synthetic lethality [32] which can be a valuable therapeutic strategy.

In this work, we expanded upon this concept and studied the consequences of transcription elongation defects on proteostasis in cancer cells with the TE^{def} phenotype. We specifically explored the adaptive pathways that TE^{def} cells use to cope with the potential lethal stress caused by their own defective transcriptional machinery. Finding therapeutic strategies for patients with TE^{def} tumors, which are inherently resistant to the current immunotherapies [10], was the main goal of this study.

We analyzed the transcriptomic profiles of several primary human breast cancers, utilized a syngeneic mouse tumor model of B16 melanoma cells treated with flavopiridol, [10] and a comprehensive *in vitro* molecular analyses of both TE^{def} and TE^{prof} breast cancer cell lines. In both human and murine models, we found that transcription defects lead to an excess of protein aggregates from likely misfolded, or otherwise aberrant, proteins. This finding is in line with the literature where aberrant transcription is often correlated with proteotoxicity [1–3,20,

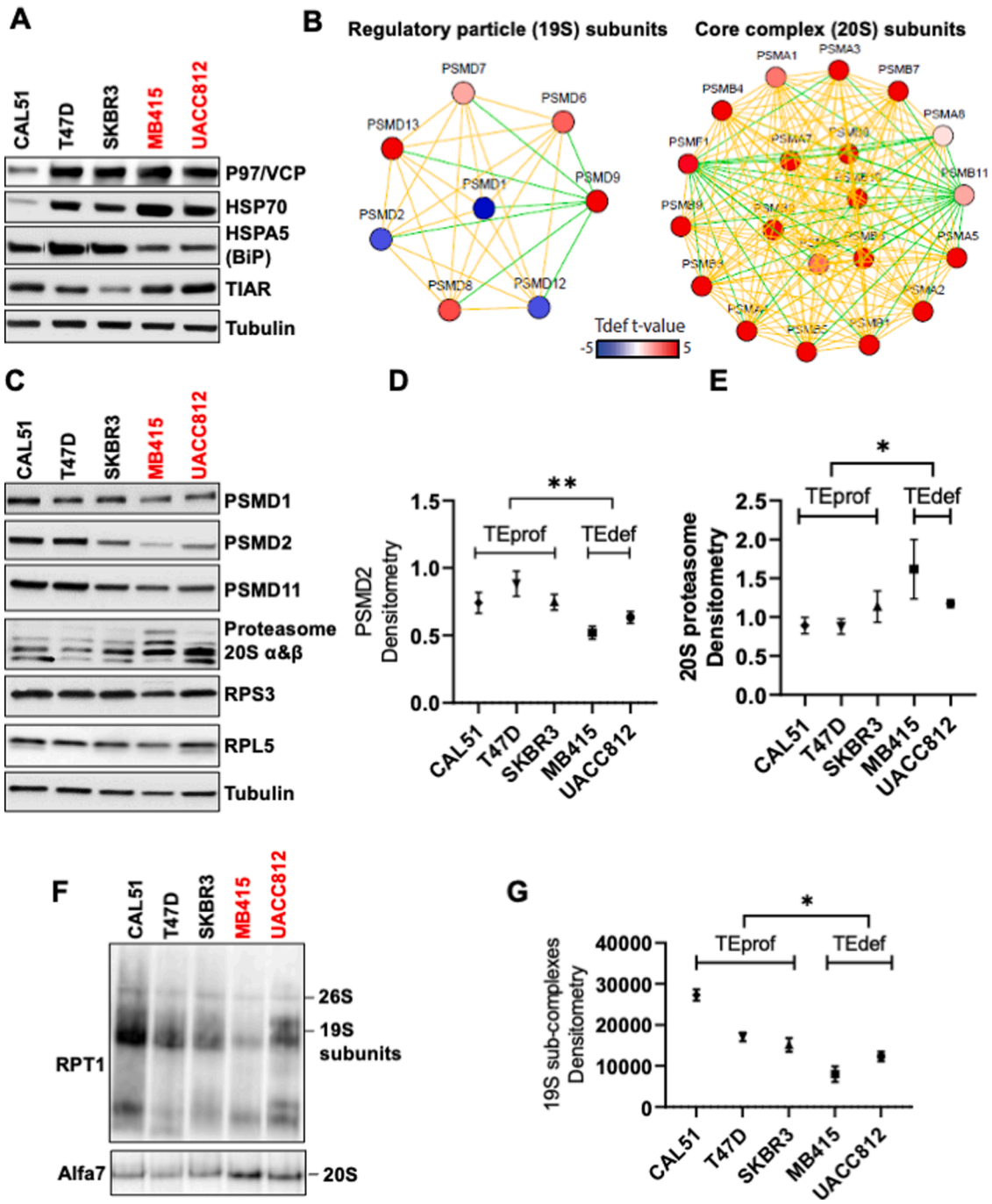

Fig. 3. Regulatory components of the proteasome system are downregulated in the TE^{def} cells: A. Immunoblots show expression levels of key proteostasis markers in control (black) versus TE^{def} (red) BC cell lines; **B.** A network view of essential components of the proteasome complex (19S and 20S particles) that are significantly suppressed/overexpressed in TE^{def} cancers in TCGA datasets. The coloring of nodes reflects the t-statistic of correlation of the mRNA expression values of corresponding genes with TE^{def} (higher value reflects higher expression in TE^{def} and vice versa); **C.** Immunoblots show expression levels of essential components of the proteasome complex in control (black) versus TE^{def} (red) BC cell lines; **D-E.** Densitometry quantification of PSMD2 and 20S proteasome subunits in **C; F.** Native gel immunoblots of proteasome subunits in control (black) versus TE^{def} (red) BC cell lines. **G.** Densitometry quantification of 19S sub-complexes shown in F. *=p<0.05 and **=p<0.01.

21]. The ubiquitin proteasome system (UPS) and autophagy are the two main interchangeable stress support pathways that cancer cells rely on to eliminate the terminally misfolded polypeptides and toxic protein aggregates [4].

It has been reported that the accumulation of toxic insoluble misfolded proteins may overwhelm the capacity of the proteasome degradation system, leading to a compromised UPS [35–37]. Compartmentalization of such aberrant proteins into protein aggregates in the cytoplasm or nucleus is viewed as a defensive and protective mechanism against stress-induced dysfunction of the UPS [12]. The proteasome complex consists of a 20S proteolytic core particle and a 19S regulatory particle. The core particle is activated for proteolysis upon its binding to one or two 19S particles to form a singly- or doubly-capped 26S proteasome complex to form the proteasome holoenzyme [14]. The 19S regulatory subunit is responsible for the recognition and substrate translocation into the lumen of the 20S core particle for

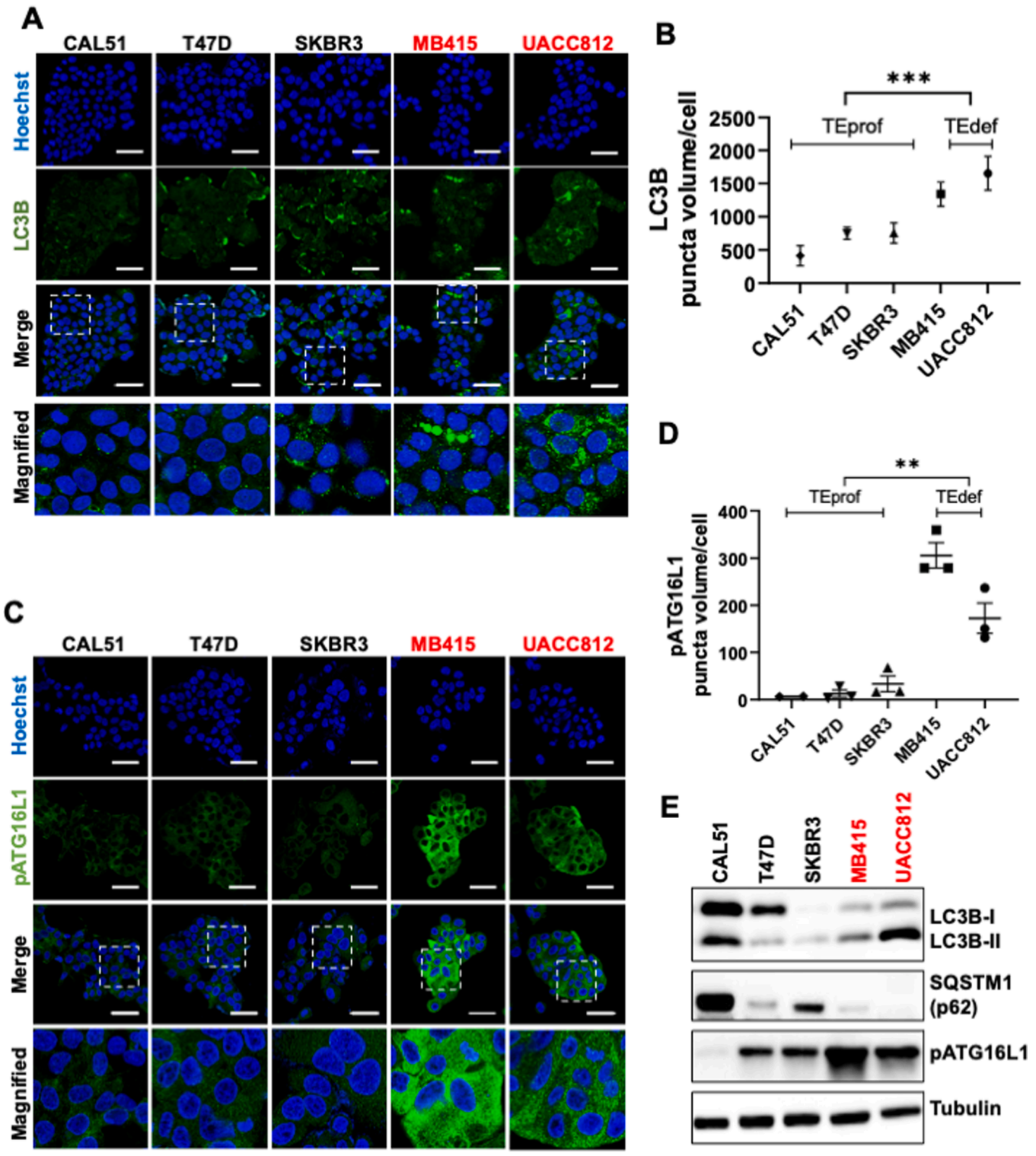

Fig. 4. TE^{def} cells upregulate markers of autophagy induction: A. Confocal images show LC3B puncta in TE^{prof} versus TE^{def} (red) BC cell lines. The bottom panel represents magnified views of the white boxed regions, scale bars; 50 μm; **B.** Quantification of LC3B puncta volume per cell calculated from 3D Z-stack confocal images in **A, C.** Confocal images of TE^{prof} (black) versus TE^{def} (red) BC cell lines stained with human pATG16L1 antibody. The bottom panel represents magnified views of the white boxed regions, scale bars; 50 μm; **D.** Quantification of pATG16L1 puncta volume per cell calculated from 3D Z-stack confocal images in **C. E.** Immunoblots show expression levels of autophagy related markers in TE^{prof} (black) versus TE^{def} (red) BC cell lines, with upregulation of LC3B-II and pATG16L1 and down-regulation of SQSTM1, which are all markers of active autophagy. **=p<0.01 and ***=p<0.001.

degradation [5,23]. Moreover, the 19S particle contains at least 18 subunits distributed over its base and lid domains which are jointly required for degradation of ubiquitinated proteins [5]. Accordingly, it has been shown that defects in the expression of 19S particles affect the proteasome activity [13]. In line with these findings, we report that essential components of the 19S regulatory subunit are downregulated in the TE^{def} cancers based on both bioinformatics and experimental analysis implying that the proteasome system is likely defective in the

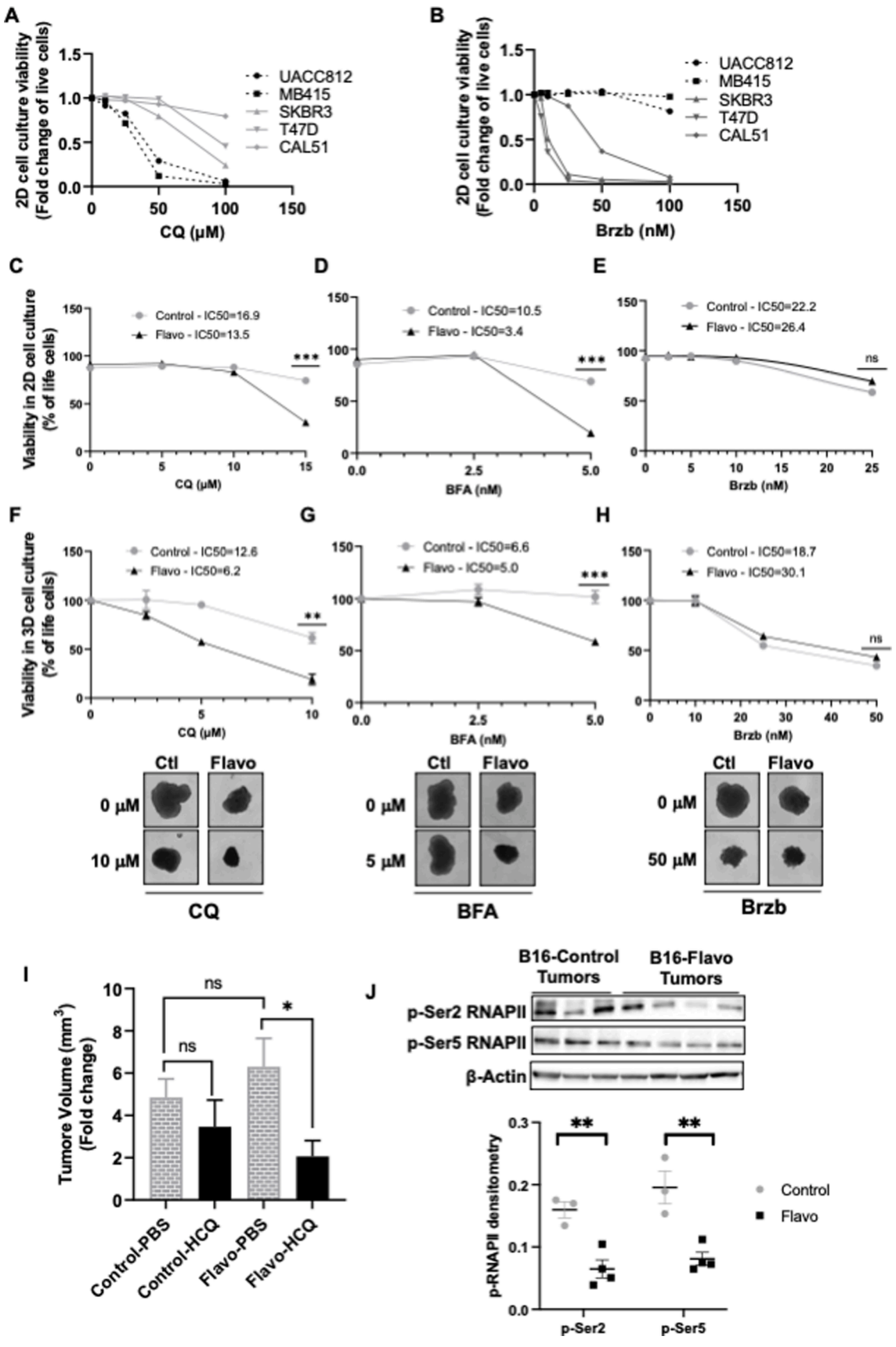

(caption on next page)

Fig. 5. TE^{def} cells are sensitive to autophagy inhibition: A-B. PI staining shows fold change of viability of control (gray) versus TE^{def} (black) BC cell lines in 2D cell culture in response to CQ and Brzb respectively; **C-E.** PI staining shows percentage of viability of control (gray) and Flavo (black) B16 cells in 2D cell culture in response to CQ, BFA, and Brzb respectively; **F-H** Luminescent assay shows percentage of viability of control (gray) and Flavo (black) B16 spheroids in 3D cell culture in response to CQ, BFA, and Brzb respectively. Representative phase contrast images of B16 tumor spheroids are represented from diluent-treated (0 μM) or drug treated cells with or without flavopiridol (Flavo) exposure. **I.** Tumor growth of control and Flavo B16 cells in C57BL/6 black mice treated with PBS or Hydroxychloroquine (HCQ). Fold change of tumor volume is presented, comparing day 11 post-treatment to day 0 of treatment. Tumors were allowed to grow one week prior to treatment with HCQ. Each group consisted of 7–16 animals. (Control-PBS $N = 7$; Control-HCQ $N = 8$; Flavo-PBS $N = 16$; Flavo-HCQ $N = 8$) **J.** Immunoblots of p-Ser2 and p-Ser5 RNAPII in tumors excised from the mice described in **I**. Each lane represents a single tumor, such that three B16-Control and four B16-Flavo tumors are shown. Densitometry values normalized to Actin are graphed below. *=$p<0.05$, **=$p<0.01$, and ***=$p<0.001$. ns=non-significant.

TE^{def} cancers. We speculate that this downregulation of 19S subunit both prevents the ubiquitinated proteins from entering the core subunit for degradation and mitigates the assembly of fully functional 26S proteasome complexes. This likely explains the abundance of ubiquitinated proteins in the insoluble fraction of the TE^{def} cell lysates.

Mechanistically, we show evidence for a significant accumulation of ubiquitinated proteins and mRNAs in the insoluble fraction of the TE^{def}, but not TE^{prof}, cells. The gene ontologies of mRNAs trapped in the insoluble fraction of TE^{def} cells overlap with gene ontologies that are suppressed in the TCGA dataset, presumably from soluble fractions, and that are associated with resistance to immunotherapy, i.e.: NFkB and Notch signaling. This suggests that the aberrant long transcripts made in TE^{def} cells are producing abnormal proteins during translation, that create protein/mRNA insoluble aggregates. Indeed, we support this view by visualizing large protein aggregates (aggresomes) in the cytoplasm of TE^{def} cells. We hypothesize that TE^{def} cells, which have impaired proteosome function, then depend upon autophagy to clear these ubiquitinated protein aggregates. Thus, inhibiting autophagy further stresses TE^{def} cells, causing decreased viability. This represents a mechanism for inducing synthetic lethality to potentially treat immunotherapy-resistant TE^{def} cancers, which comprise about 15-25% of all cancers. This is supported by our findings using 2D cultures, 3D spheroid cultures, and syngeneic, immunocompetent grafted tumor models. Using both genetic and small molecule inhibitor models, TE^{def} cancers treated with autophagy inhibitors have decreased viability *in vitro* and impaired tumor growth *in vivo* compared to TE^{prof} controls. Further work is necessary to determine if the protein/mRNA aggregates in TE^{def} cells indeed consist of translation machinery products or proteins produced from aberrant transcripts originated from the defective transcription elongation phenotype.

One limitation of this report is the focus solely on breast cancers, while the TE^{def} phenotype has been noted in multiple solid tumor types and in hematological malignancies. Therefore, additional work is needed to determine if sensitivity to autophagy inhibition is observed in TE^{def} tumors originating from other tissues. An additional limitation is that we have tested only a limited number of small molecules from various drug classes (i.e.: aphidicolin for genomic stress, bortezomib for proteosome inhibition, chloroquine for autophagy inhibition). Thus, more work is required to test if TE^{def} tumors are differentially sensitive to other drugs and drug classes beyond those tested here, despite their universal resistance to immunotherapy. Finally, we have not yet elucidated the molecular mechanism driving the TE^{def} phenotype, and it is unknown if the flavopiridol-mediated suppression of CDK9 fully recapitulates the TE^{def} phenotype observed in patient samples.

Combined, we are the first to report that TE^{def} tumors undergo chronic proteotoxic stress, likely due to the production of misfolded proteins translated from aberrant transcripts. We then go on to identify a unique vulnerability through a dependency upon autophagy for TE^{def} cancer cell survival, which can be exploited to improve treatment outcomes.

Conclusions

We posit that high levels of protein aggregates and dysfunctionality of the 26S proteasome complex pushes TE^{def} cancer cells toward autophagy addiction. Accordingly, blocking the autophagy pathway maximizes proteotoxic stress, due to the accumulation of toxic protein aggregates derived from the spurious defective transcripts, leading to a strong synthetic lethality which can be exploited for therapeutic purposes.

Data availability statement

Publicly available datasets were analyzed in this study and acquired from The Cancer Genome Atlas (TCGA). Data from TCGA can be accessed here: https://portal.gdc.cancer.gov/ Additional raw data for this study were generated at the Genomics, Epigenomics, and Sequencing Core at the University of Cincinnati. Derived data supporting the findings of this study are available from the corresponding author upon request.

CRediT authorship contribution statement

B. Muhammad: Conceptualization, Methodology, Validation, Formal analysis, Investigation, Writing – original draft, Funding acquisition. **L.G. Parks:** Investigation, Writing – review & editing. **K. Komurov:** Conceptualization, Software, Validation, Supervision, Funding acquisition. **L.M. Privette Vinnedge:** Validation, Writing – review & editing, Supervision, Funding acquisition.

Declaration of Competing Interest

The authors declare the following financial interests/personal relationships which may be considered as potential competing interests: Co-author Kakajan Komurov is currently employed by Champions Oncology, Inc.

Acknowledgements

This research was funded by grant numbers [R37-CA218072] (LMPV) and [R01-CA193549] (KK and LMPV) from the National Cancer Institute of the United States National Institutes of Health. Additional funding was provided by the CancerFree KIDS Foundation (BM). All flow cytometric data were acquired using equipment maintained by the Research Flow Cytometry Core in the Division of Rheumatology at Cincinnati Children's Hospital Medical Center and with the assistance of Core staff. We also acknowledge the assistance of Victoria Summey with the Comprehensive Mouse and Cancer Core and John Matthew ("Matt") Kofron of the Confocal Imaging Core at Cincinnati Children's Hospital Medical Center.

Supplementary materials

Supplementary material associated with this article can be found, in the online version, at doi:10.1016/j.tranon.2021.101323.

References

[1] D. Balchin, M. Hayer-Hartl, F.U. Hartl, *In vivo* aspects of protein folding and quality control, Science 353 (6294) (2016) aac4354.
[2] M.H.Z. Guang, et al., Targeting proteotoxic stress in cancer: a review of the role that protein quality control pathways play in oncogenesis, Cancers (Basel) 11 (1) (2019).

[3] J.T. Wade, D.C. Grainger, Spurious transcription and its impact on cell function, Transcription 9 (3) (2018) 182–189.
[4] S. Wolff, J.S. Weissman, A. Dillin, Differential scales of protein quality control, Cell 157 (1) (2014) 52–64.
[5] S. Alberti, et al., Granulostasis: protein quality control of RNP granules, Front. Mol. Neurosci. 10 (2017) 84.
[6] U.B. Pandey, et al., HDAC6 rescues neurodegeneration and provides an essential link between autophagy and the UPS, Nature 447 (7146) (2007) 859–863.
[7] T. Hara, et al., Suppression of basal autophagy in neural cells causes neurodegenerative disease in mice, Nature 441 (7095) (2006) 885–889.
[8] M. Komatsu, et al., Impairment of starvation-induced and constitutive autophagy in Atg7-deficient mice, J. Cell Biol. 169 (3) (2005) 425–434.
[9] Z. Yang, D.J. Klionsky, An overview of the molecular mechanism of autophagy, Curr. Top. Microbiol. Immunol. 335 (2009) 1–32.
[10] V. Modur, et al., Defective transcription elongation in a subset of cancers confers immunotherapy resistance, Nat. Commun. 9 (1) (2018) 4410.
[11] K. Komurov, et al., NetWalker: a contextual network analysis tool for functional genomics, BMC Genom. 13 (2012) 282.
[12] C.M. Maghames, et al., NEDDylation promotes nuclear protein aggregation and protects the ubiquitin proteasome system upon proteotoxic stress, Nat. Commun. 9 (1) (2018) 4376.
[13] A. Levin, et al., PSMD5 inactivation promotes 26S proteasome assembly during colorectal tumor progression, Cancer Res. 78 (13) (2018) 3458–3468.
[14] H.C. Tai, et al., Characterization of the brain 26S proteasome and its interacting proteins, Front. Mol. Neurosci. 3 (2010) 1–12.
[15] S. Elsasser, M. Schmidt, D. Finley, Characterization of the proteasome using native gel electrophoresis, Ubiquitin Protein Degrad. Part A 398 (2005) 353–363.
[16] L.C. Crowley, et al., Measuring cell death by propidium iodide uptake and flow cytometry, Cold Spring Harb. Protoc. 2016 (7) (2016) 647–651.
[17] S. Namkoong, et al., Systematic characterization of stress-induced RNA granulation, Mol. Cell 70 (1) (2018) 175–187, e8.
[18] D.M. Euhus, et al., Tumor measurement in the nude mouse, J. Surg. Oncol. 31 (4) (1986) 229–234.
[19] M.M. Tomayko, C.P. Reynolds, Determination of subcutaneous tumor size in athymic (nude) mice, Cancer Chemother. Pharmacol. 24 (3) (1989) 148–154.
[20] J.A. Johnston, C.L. Ward, R.R. Kopito, Aggresomes: a cellular response to misfolded proteins, J. Cell Biol. 143 (7) (1998) 1883–1898.
[21] K. Bersuker, M. Brandeis, R.R. Kopito, Protein misfolding specifies recruitment to cytoplasmic inclusion bodies, J. Cell Biol. 213 (2) (2016) 229–241.
[22] I. Amm, T. Sommer, D.H. Wolf, Protein quality control and elimination of protein waste: the role of the ubiquitin-proteasome system, Biochim. Biophys. Acta 1843 (1) (2014) 182–196.
[23] M. Rechsteiner, C.P. Hill, Mobilizing the proteolytic machine: cell biological roles of proteasome activators and inhibitors, Trends Cell Biol. 15 (1) (2005) 27–33.
[24] N.M. Kocaturk, D. Gozuacik, Crosstalk between mammalian autophagy and the ubiquitin-proteasome system, Front. Cell Dev. Biol. 6 (2018) 1–27.
[25] W. Tian, et al., An antibody for analysis of autophagy induction, Nat. Methods 17 (2) (2020) 232–239.
[26] P. Li, et al., Chloroquine inhibits autophagy and deteriorates the mitochondrial dysfunction and apoptosis in hypoxic rat neurons, Life Sci. 202 (2018) 70–77.
[27] C. Verbaanderd, et al., Repurposing drugs in oncology (ReDO)-chloroquine and hydroxychloroquine as anti-cancer agents, Ecancermedicalscience 11 (2017) 1–35.
[28] C.I. Chude, R.K. Amaravadi, Targeting autophagy in cancer: update on clinical trials and novel inhibitors, Int. J. Mol. Sci. 18 (6) (2017) 1–11.
[29] S.B. Goldberg, et al., A phase I study of erlotinib and hydroxychloroquine in advanced non-small-cell lung cancer, J. Thorac. Oncol. 7 (10) (2012) 1602–1608.
[30] R.K. Amaravadi, et al., Autophagy inhibition enhances therapy-induced apoptosis in a Myc-induced model of lymphoma, J. Clin. Investig. 117 (2) (2007) 326–336.
[31] M. Vermulst, et al., Transcription errors induce proteotoxic stress and shorten cellular lifespan, Nat. Commun. 6 (2015) 8065.
[32] J. Luo, N.L. Solimini, S.J. Elledge, Principles of cancer therapy: oncogene and non-oncogene addiction, Cell 136 (5) (2009) 823–837.
[33] Y.A. Fouad, C. Aanei, Revisiting the hallmarks of cancer, Am. J. Cancer Res. 7 (5) (2017) 1016–1036.
[34] I. Caon, et al., Revisiting the hallmarks of cancer: the role of hyaluronan, Semin. Cancer Biol. 62 (2020) 9–19.
[35] N.F. Bence, R.M. Sampat, R.R. Kopito, Impairment of the ubiquitin-proteasome system by protein aggregation, Science 292 (5521) (2001) 1552–1555.
[36] P. Deriziotis, et al., Misfolded PrP impairs the UPS by interaction with the 20S proteasome and inhibition of substrate entry, EMBO J. 30 (15) (2011) 3065–3077.
[37] E. Lindersson, et al., Proteasomal inhibition by alpha-synuclein filaments and oligomers, J. Biol. Chem. 279 (13) (2004) 12924–12934.